JGR Solid Earth

RESEARCH ARTICLE
10.1029/2025JB032433

The Influence of Elevated Temperature on Time-Dependent Compaction Creep in Bleursville Sandstone

Mark Jefferd[1,2,3], **Nicolas Brantut**[3,4], **Thomas M. Mitchell**[3], **and Philip G. Meredith**[3]

[1]Department of Earth Sciences, Utrecht University, Utrecht, The Netherlands, [2]Faculty of Geo-information Science and Earth Observation (ITC), University of Twente, Enschede, The Netherlands, [3]Department of Earth Sciences, University College London, London, UK, [4]GFZ German Centre for Geosciences, Potsdam, Germany

Abstract The inelastic compaction of sandstone in the upper crust typically occurs at depths where temperatures range from approximately 50°C to 150°C. Previous experimental studies have shown that even this modest temperature increase can reduce the yield stress required to initiate inelastic compaction, and can also enhance time-dependent deformation within the brittle regime. However, the influence of these realistic crustal temperatures on sandstone compaction over longer time scales has not yet been systematically explored. We performed triaxial creep experiments on Bleursville sandstone at an effective pressure of 100 MPa and at temperatures of either room temperature, 75°C, or 150°C. Our results show that the differential stress required to initiate creep is up to 20 MPa lower at 150°C than at room temperature. In addition, at any given differential stress, axial creep strain rates were more than an order of magnitude higher at 150°C.We also find that the typical decrease in strain rate with increasing axial strain was less pronounced at higher temperatures. This indicates that the stress sensitivity of the creep rate is reduced as temperature increases. Finally, we extrapolated our experimentally derived creep laws for Bleursville sandstone and combined them with theoretical estimates of pressure-solution rates at lower stresses and strain rates. This shows that time-dependent deformation at room temperature is dominated by subcritical cracking across all conditions examined. In contrast, at 150°C, Bleursville sandstone may begin to deform by pressure solution once strain rates fall below approximately 10^{-9} s^{-1}.

Plain Language Summary In the Earth's crust, sandstones can deform and become more compact under pressure. As temperature increases with depth, this compaction often occurs at temperatures between 50°C and 150°C. Most previous experiments have studied sandstone compaction at room temperature. However, it remains unclear how increased temperature affects sandstone compaction, especially over longer timescales, which are important for many geological processes. To investigate this, we carried out laboratory experiments using Bleursville sandstone. We applied pressure and heated the rock to room temperature, 75°C, or 150°C. We found that at 150°C, the sandstone was weaker and began to compact under lower stress compared to room temperature. This weakening effect became even more pronounced in longer experiments. We conclude that the increased weakening of sandstone over longer timescales at higher temperatures is likely due to chemical reactions between the rock and the water.

Key Points:

- The creep strain rate is an order of magnitude higher at 150°C compared to room temperature at a given stress
- An elevated temperature reduces the stress required for time-dependent inelastic sandstone deformation
- The stress dependence on the creep strain rate is lowered at an elevated temperature of 150°C

Correspondence to:
M. Jefferd,
m.a.jefferd@uu.nl

Citation:
Jefferd, M., Brantut, N., Mitchell, T. M., & Meredith, P. G. (2026). The Influence of elevated temperature on time-dependent compaction creep in Bleursville sandstone. *Journal of Geophysical Research: Solid Earth*, *131*, e2025JB032433. https://doi.org/10.1029/2025JB032433

Received 23 JUL 2025
Accepted 24 DEC 2025
Corrected 2 MAR 2026

This article was corrected on 2 MAR 2026. See the end of the full text for details.

Author Contributions:
Conceptualization: Mark Jefferd, Nicolas Brantut
Formal analysis: Mark Jefferd
Funding acquisition: Mark Jefferd, Nicolas Brantut
Investigation: Mark Jefferd
Methodology: Mark Jefferd, Thomas M. Mitchell
Project administration: Mark Jefferd, Nicolas Brantut
Resources: Thomas M. Mitchell, Philip G. Meredith
Supervision: Nicolas Brantut, Thomas M. Mitchell, Philip G. Meredith
Visualization: Mark Jefferd
Writing – original draft: Mark Jefferd
Writing – review & editing: Mark Jefferd, Nicolas Brantut, Thomas M. Mitchell, Philip G. Meredith

1. Introduction

The inelastic compaction of sandstone corresponds to a permanent reduction in porosity, which can alter the physical, chemical, and transport properties of the rock. Sandstone compaction can occur naturally or as a result of anthropogenic influences on the subsurface, such as resource extraction or fluid injection. It is therefore observed across a wide range of geological settings, environmental conditions, and time spans. The natural diagenesis and/or the slow porosity reduction of porous rocks due to fluid-assisted, stress-driven mass transfer may operate over time scales ranging from thousands to millions of years (Gratier et al., 1999; Rutter, 1976; Spiers et al., 2003). In contrast, compaction in reservoir settings due to the human-driven pore fluid extraction typically operates over decades (Martin & Serdengecti, 1984; Pijnenburg et al., 2018; Shinohara et al., 2024), while compaction in fault damage zones may occur even more rapidly, with dynamic compaction bands forming during seismic events (Aben et al., 2017; Bésuelle & Rudnicki, 2004).

The macroscopic impact of sandstone compaction is evident in phenomena such as surface subsidence above reservoirs (Fredrich et al., 2000; Geertsma et al., 1973) and the formation of compaction bands observed in the

field (Fossen et al., 2007). These large-scale manifestations are inherently governed by micro-mechanical deformation mechanisms, including grain fracturing (Baud et al., 2000; Heap et al., 2015; Wong et al., 1997), slip at grain interfaces (Bernabe et al., 1994; Menéndez et al., 1996), plastic deformation of clay fractions (Pijnenburg et al., 2018, 2019a), and dissolution-precipitation processes (Niemeijer et al., 2002). While applied stress is the primary control on these mechanisms, environmental factors such as temperature and fluid and rock chemistry may also exert an important influence.

The complexity of these microscale processes can result in time-dependent compaction behavior. Such time dependency may arise from two nonexclusive end-member scenarios: (a) time-dependent stress evolution, for example, tectonic loading or fluid withdrawal/injection, leading to instantaneous inelastic deformation, or (b) time-dependent creep under constant applied stresses that originates from processes such as subcritical cracking and dissolution-precipitation, where deformation may continue with increasing time (Brantut et al., 2013). In sandstones, creep and stress relaxation experiments have shown that time-dependent inelastic deformation can occur in the macroscopically brittle regime (dilatant behavior) (Heap, Baud, Meredith, Bell, & Main, 2009; Jiang et al., 2013; Ngwenya et al., 2001; Shengqi & Jiang, 2010) and also in the macroscopically ductile regime (compactive behavior) (Heap et al., 2015; Pijnenburg et al., 2018).

In situations where grain fracturing is the dominant microscale phenomenon driving deformation, time-dependent deformation is often attributed to subcritical crack growth (Brantut et al., 2013). Subcritical crack growth occurs as a result of chemical interactions between a reactive agent and the grain material of a stressed crack tip. These chemical interactions act to weaken the chemical bonds at the crack tip which enables crack propagation at lower applied stresses. The process of bond weakening is known as stress corrosion and in sandstones the primary chemical interactions are thought to occur between quartz and water (Scholz, 1972). Subcritical cracking potentially impacts the minimum stress level required for the onset of inelastic deformation. It has been demonstrated theoretically and experimentally that microcracks within rocks (or individual grains) will readily grow in the presence of a chemically active fluid at stress levels below the perceived critical limit through subcritical cracking (Anderson & Grew, 1977; Atkinson & Meredith, 1987; Lawn, 1993). Subcritical crack growth rates are highly sensitive to the applied stress, chemical environment and temperature (Lawn, 1993), and all these factors have been shown to impact the time-dependent deformation of sandstones in the brittle creep regime (Brantut et al., 2013).

In the compactive regime, experimental data on time-dependent deformation of sandstone remain limited. Existing studies nevertheless indicate that compaction can be strongly rate dependent. Heap et al. (2015) showed that localized compaction bands in Bleurswiller sandstone may form in a time-dependent manner, with deformation rates controlled by applied stress in a way comparable to that observed in the brittle (dilatant) creep regime. Subsequent constant strain rate (CSR) experiments demonstrated that Bleurswiller sandstone exhibits a reduction in peak strength at lower loading rates (Shinohara et al., 2024). The commonly assumed chemically driven nature of rate-dependent compactive deformation suggests that environmental factors may also exert an important control on deformation rates. However, the influence of such factors, temperature in particular, has not yet been systematically investigated. The potential importance of environmental controls is highlighted by the work of Schimmel et al. (2022), who showed that pore fluid chemistry strongly affects uniaxial compaction in Bentheim sandstone, with aqueous alkaline fluids promoting time-dependent compaction.

At the crustal depths relevant to sandstone compaction, typically between 1 and 6 km, ambient temperature ranges from 35°C to 200°C, depending on the local geotherm. Within this temperature range, recent experimental work has shown that increasing the temperature from room temperature to 150°C weakens sandstones in the ductile regime and to a lesser degree the brittle regime in short duration experiments (at strain rates of the order of 10^{-5} s^{-1}, (Jefferd et al., 2021)). In the compactive regime, three different sandstones experienced a reduction in the differential stress required to cause inelastic compaction by 10%–30%, and there was also a reduction in the hydrostatic grain crushing pressure, P^*, by about 10%. The overall weakening at elevated temperature was attributed to a combination of a reduction in fracture toughness and a potential slight increase in the rate of subcritical cracking (Jefferd et al., 2021).

While the weakening effect of temperature in the presence of pore water is well established for short-term, constant strain-rate experiments. The influence of elevated temperature on the time-dependent compaction behavior of sandstone remains poorly constrained. Experiments conducted in the brittle creep regime have

demonstrated that a temperature increase from room temperature to 75°C increases the strain rate at a given applied stress by 2–3 orders of magnitude (Heap, Baud, & Meredith, 2009). If the underlying creep processes in the compaction creep regime are similar to those in the brittle creep regime, we also expect similarities in the macroscopic temperature dependency of creep rates. An additional mechanism that could be expected to play a role during compaction creep, especially at elevated temperature, is intergranular pressure solution. This mechanism has been evidenced in high temperature (150°C) laboratory experiments on quartz aggregates (e.g., (Dewers & Hajash, 1995; Niemeijer et al., 2002; Schutjens et al., 2021)), but its contribution to deformation in consolidated sandstone is not yet clear.

Here, we aim to determine the effect of temperature on the rate of time-dependent deformation in the compactive deformation regime of sandstone. We conducted triaxial CSR and creep (constant stress) experiments on Bleursville sandstone, and measured the impact of temperature change on creep deformation rate and its stress dependency. We construct an empirical relationship between applied stress, temperature and creep rate for Bleursville sandstone and include including predictions from intergranular pressure solution. At 150°C and strain rates above 10^{-9} s^{-1}, we find that creep is most likely driven by subcritical cracking.

2. Sample Material and Apparatus

The sandstone used was Bleursville sandstone from Bleurville, Vosges, north-eastern France. This pale beige colored sandstone has a starting porosity of 22.7% (±1.5%, measured with a helium pycnometer) and is composed of 81 ± 2% quartz, 12% feldspar and 7 ± 2% mica. Its grains are spherical to sub-spherical and have a reasonably uniform diameter of about 0.12 mm. Earlier studies on Bleurswiller sandstone (a sandstone from a different area of the quarry Bleursville sandstone comes from) have demonstrated that there is a transition from dilational to compactive deformation at effective pressures above approximately 40–50 MPa (Baud et al., 2015; Fortin et al., 2005; Heap et al., 2015). Cylindrical samples were cored from a single block perpendicular to the sedimentary bedding, and the ends were ground flat. The final length of the samples was 52 mm and the diameter was 25 mm. Each sample was then washed with distilled water before being oven dried at 60°C for a minimum of 48 hr.

Experiments were performed using a conventional triaxial deformation apparatus in the Rock and Ice Physics Laboratory at University College London. For a detailed description of the apparatus refer to Jefferd et al. (2021). In brief, the triaxial rig operates by placing the rock sample in a rubber jacket and attaching the sample to a piston assemblage, both of which are then placed inside a cylindrical pressure vessel. A confining pressure of up to 120 MPa can be applied to the sample by pressurizing silicone oil inside the pressure vessel using a servo-controlled hydraulic intensifier. With the sample separated from the confining fluid through the rubber jacket, a pore pressure can then be imposed on the sample by using a separate servo-controlled hydraulic intensifier. Both the confining pressure and pore pressure can be maintained at a constant value for the duration of the experiment, with a maximum deviation of ±0.1 MPa from the set point. An internal Linear Variable Differential Transformer (LVDT) inside the pore pressure intensifier allows for the continuous monitoring of the reservoir volume of the intensifier, which in turn is used to measure the porosity change of the sample.

The pressure vessel is located inside a 2,600 kN hydraulically operated loading frame, which can supply an axial force to the sample through a servo-controlled hydraulic piston. The axial load can be applied by operating the piston in two distinct modes. The first operational mode involves moving the piston at a constant set displacement rate (strain rate) and measuring the load required to maintain the constant rate of displacement. The second operational mode is when the piston is placed in load control. In this mode, a target force is set and the piston will continue to move axially to maintain the target force. In both modes the axial displacement is measured during the experiment using an external LVDT and the axial load is measured using an external load cell. If required, the whole pressure vessel and sample can be heated by three external band heaters to a maximum temperature of 250°C.

3. Experimental Procedure

To evaluate how elevated temperature affects the rate of time-dependent sandstone compaction, triaxial creep experiments were performed. To ensure that the samples were in the fully compactive regime an effective pressure of 100 MPa was used for all experiments.

Table 1
Summary of Experimental Conditions

Experiment Number	Temperature (°C)	Type of experiment	Diff. Stress (es) during creep (MPa)	Max. Strain (%)
Bleursville Sandstone, Effective Pressure = 100 MPa				
1	20	Single stress	93	5.1
2	150	Single stress	78	4.8
3	20	Single stress	77	2.2
4	75	Single stress	66	4.3
5	150	Single stress	66	5.2
6	20	Stress stepping	54, 64, 75, 85, 95	4.1
7	75	Stress stepping	58, 68, 78	4.4
8	150	Stress stepping	53, 63	4.1

Before each experiment, the sample was saturated with distilled water under vacuum for at least 2 hr and all experiments were performed with distilled water as the starting pore fluid. The saturated sample was fitted into a rubber jacket and placed inside the triaxial machine. The confining pressure was then applied, initially by means of a hand pump to a value of 8 MPa, which was then maintained by the servo-controlled intensifier. A pore pressure of 5 MPa was then applied at a rate of 0.05 MPa s^{-1} and the sample was allowed to fully resaturate at these pressures. The sample was considered to be fully saturated when the pore pressure intensifier volume ceased to change. For experiments performed at elevated temperature, external heaters were then turned on to warm the sample at an average heating rate of approximately 0.5°C min^{-1}. Experiments were primarily carried out at room temperature or at 150°C, with a few additional experiments carried out at 75°C. In total it took approximately 5 hr for the system to reach equilibrium at 150°C. Once the system had reached the target temperature, the confining pressure was then increased to 105 MPa at a rate of 0.05 MPa s^{-1} and left for a minimum of 2 hr to achieve pressure and temperature equilibrium.

An axial differential stress was then applied by loading at a constant axial strain rate of 10^{-5} s^{-1}, until a target level of differential stress was achieved (as summarised in Table 1). Creep was then initiated by holding the stress constant for a period of time. In this study, two different styles of creep test were performed: (a) single stress level creep tests, which is when the differential stress is held constant until a target axial strain level was reached (maximum 5% axial strain) and (b) stress stepping creep tests, where if at any point during the creep phase the axial strain rate decreased to approximately 10^{-8} s^{-1} either a stress step increase of 10 MPa was applied or the experiment was ended. The stress stepping technique is similar to that employed by Heap, Baud, Meredith, Bell, and Main (2009); Heap et al. (2015) and it has the advantage of being able to gather data at multiple stress levels on the same sample, therefore negating the issue of sample variability if multiple single stress level tests were done. It is important to note however, that during a stress stepping experiment the starting strain of each step and therefore the micro-structural state of the sample will be slightly different for each stress step. In total, the experiments varied in duration from a few days to a few weeks. At the end of the creep phase the axial load was removed, followed by the lowering of the confining and pore pressures in a step wise manner. The external heaters were then turned off and the whole vessel was allowed to cool before the sample was removed.

4. Results

To compare the various creep tests to one another, it is useful to include a reference CSR experiment at each creep temperature used. During a CSR experiment the piston is advanced at a constant rate and the corresponding axial stress is recorded. The CSR experiments presented (Figure 1a) are the same as those described by Jefferd et al. (2021), and initially show a linear increase in differential stress with axial strain. A deviation away from linearity in the pore volume data was used by Jefferd et al. (2021) to deduce the onset of macroscopic inelastic compaction (C^*) at an effective pressure of 100 MPa occurred at 63 and 48 MPa at room temperature and 150°C respectively. With increasing axial strain a rollover stress point was observed, with a small plateau in the stress being subsequently reached, before strain hardening continues until the termination of the experiment. Increasing the temperature from room temperature to 150°C reduces the plateau stress by about 15 MPa. At 75°C the

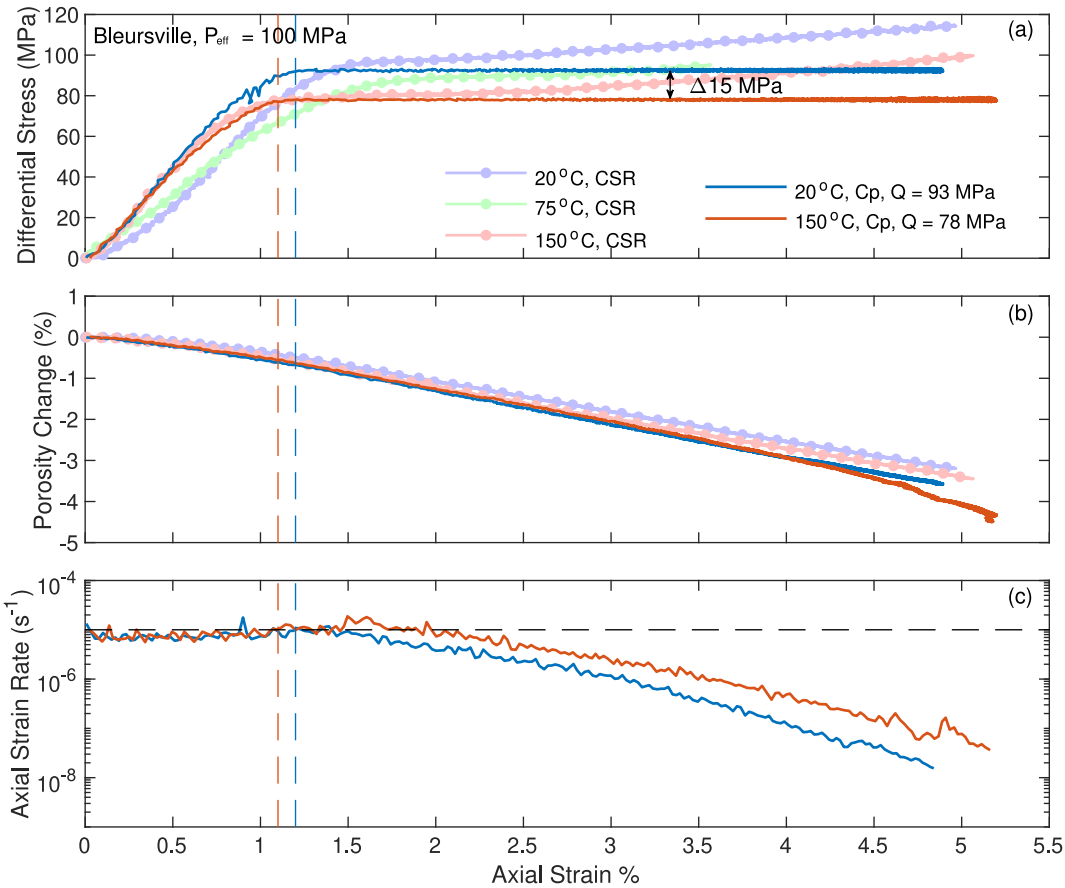

Figure 1. (a) Differential stress against axial strain for three constant strain rate (CSR) tests (dots) and two creep (Cp) tests (line), at 150°C (red), and room temperature (blue). The stress level of the creep experiments closely matches the plateau stress of the CSR tests. (b) Porosity change against axial strain for the experiments depicted in (a). A negative porosity reduction indicates compaction. (c) Axial strain rate as a function of axial strain for the creep experiments shown in (a). The black dashed line indicates a strain rate of 10^{-5} s^{-1} which is the strain rate of CSR experiments and the loading phase of the creep experiments. In all figure parts the dotted vertical line indicates the onset of creep.

differential stress plateau occurred at 90 MPa, which is in between the 97 MPa plateau seen at room temperature and the 80 MPa plateau seen at 150°C.

The differential stress levels for the highest stress creep experiments were picked to match the onset of the differential stress plateaus observed during the CSR loading phase of each experiment, which resulted in a creep stress of 93 MPa at room temperature and 78 MPa at 150°C (Figure 1a). The measurements of porosity change (Figure 1b) show that all samples experienced compaction for the duration of the experiment and the total porosity reduction was between 3% and 4% for all tests. The axial strain rate for the creep experiments initially remained close to the value of 10^{-5} s^{-1} imposed during loading, up to 0.3% axial strain at room temperature and up to 0.8% strain at 150°C. The strain rate then decreased in a log-linear manner with increasing axial strain, so that the strain rate at 4.8% axial strain was 1×10^{-8} s^{-1} at room temperature and 7×10^{-8} s^{-1} at 150°C (Figure 1c).

When the creep stress was set as low as 80% of the plateau stress (Figure 2), the strain rate during creep no longer decreased in a log-linear manner with increasing axial strain (Figure 2c). At room temperature, the strain rate rapidly decreased from 10^{-5} s^{-1} at the onset of creep to 1×10^{-8} s^{-1} in just 0.7% axial strain. The rate of porosity reduction of the room temperature test was greatly reduced for the last 0.5% axial strain. It is not clear what caused this observation and as the effect only appears minor, it will not be interpreted further (Figure 2b). For the experiment performed at 150°C and 80% of the plateau stress, the strain rate reduced to 10^{-6} s^{-1}, where it remained relatively constant for a further 2% axial strain, before decreasing in a log-linear manner to 4×10^{-8} s^{-1}

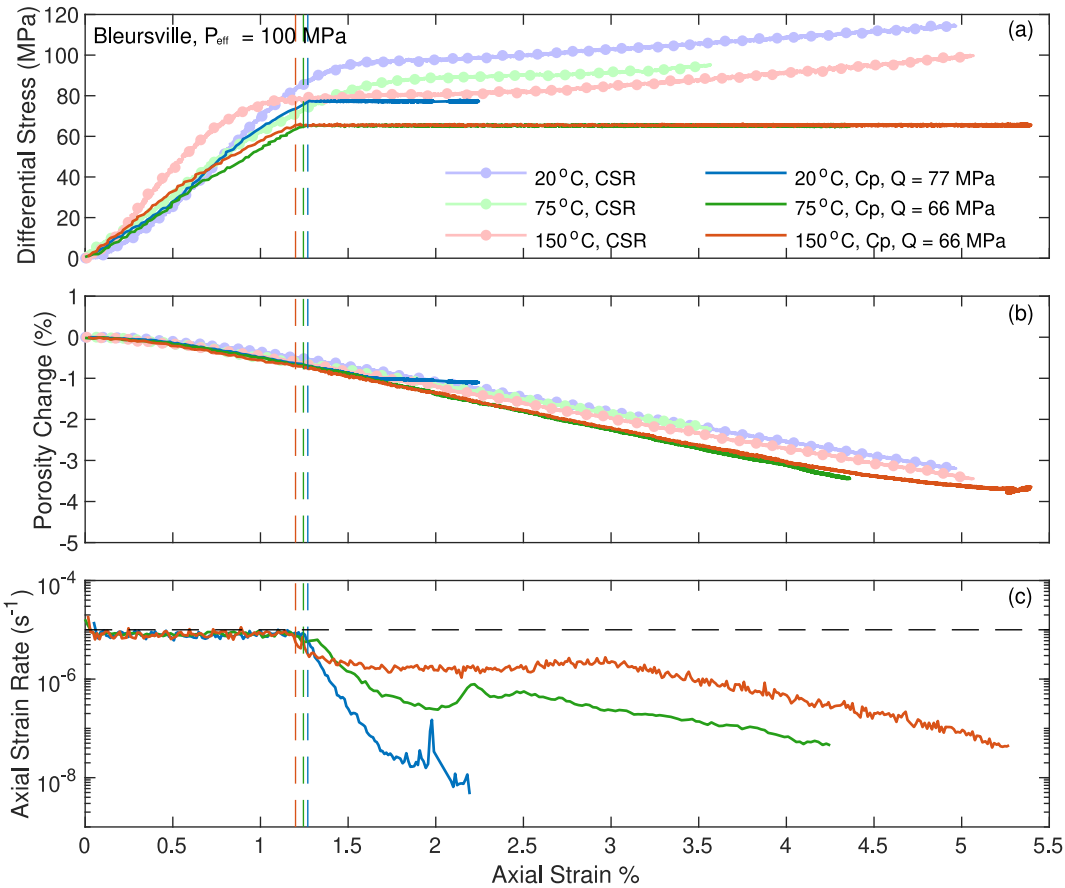

Figure 2. (a) Differential stress against axial strain for three constant strain rate (CSR) tests (dots) and three creep tests (line), at 150°C (red), 75°C (green) and room temperature (blue). (b) Porosity change against axial strain for the experiments depicted in (a). A negative porosity reduction indicates compaction. (c) Axial strain rate as a function of axial strain for the creep experiments shown in (a). The black dashed line indicates a strain rate of 10^{-5} s^{-1} which is the strain rate of CSR experiments and the loading phase of the creep experiments. In all figure parts the dotted vertical line indicates the onset of creep.

at 5% axial strain (Figure 2c). In contrast to the room temperature and 150°C experiments, the creep experiment performed at 75°C was carried out at the same differential stress (66 MPa) as the 150°C experiment instead of 80% of the plateau stress. The creep strain rate at 75°C also reduced at the onset of creep, at a rate between that of the room temperature and 150°C tests. At approximately 2% axial strain, the 75°C test experienced a transient strain rate increase by about half an order of magnitude before continuing to reduce, so that after 4.5% axial strain the sample was creeping at a strain rate of 4×10^{-8} s^{-1} (Figure 2c), which is between the room temperature and the 150°C test results.

For the stress stepping experiments (Figure 3), the first differential stress used was 55 MPa (±2 MPa) and this was increased by 10 MPa increments whenever the strain rate dropped below approximately 10^{-8} s^{-1}, until about 4% axial strain was accumulated. The stress steps were performed at a loading rate which was approximately equal to 10^{-5} s^{-1} and were therefore reflected as spikes in the strain rate evolution plotted against axial strain (Figure 3c). The samples deformed at room temperature and 75°C experienced porosity reduction with increasing axial strain at a similar rate to the samples deformed at CSR. The sample deformed at 150°C experienced more volumetric compaction than those deformed at lower temperature, but it is not clear what caused this difference.

The strain rate for the room temperature test (Figure 3c) dropped to 10^{-8} s^{-1} after about 0.3% axial strain past the start of the first creep phase. Two further stress increases of 10 MPa yielded very similar strain rate evolutions, where after approximately 0.3% strain the strain rate decreased to 10^{-8} s^{-1}. Only after the third stress step to a differential stress of 75 MPa did the strain rate stay above 10^{-8} s^{-1} for a larger amount of axial strain. At 1.7% axial strain, a transient increase was observed in the strain rate. Another stress step was performed at 2.5% axial

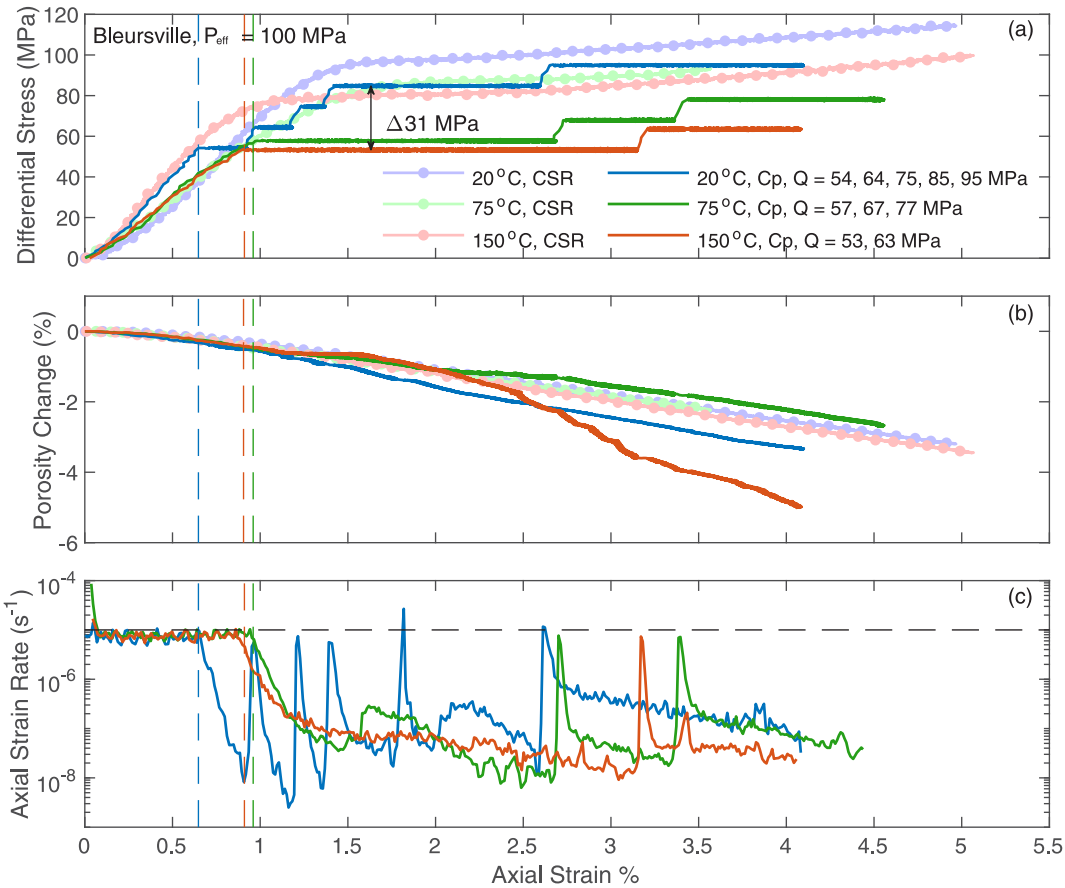

Figure 3. (a) Differential stress against axial strain for three constant strain rate (CSR) tests (dots) and three creep tests (line), at 150°C (red), 75°C (green) and room temperature (blue). (b) Porosity change against axial strain for the experiments depicted in (a). A negative porosity reduction indicates compaction. (c) Axial strain rate as a function of axial strain for the creep experiments shown in (a). The black dashed line indicates a strain rate of 10^{-5} s^{-1} which is the strain rate of the CSR experiments and the loading phase of the creep experiments. In all panels, the dotted vertical line indicates the onset of creep.

strain, after which we observed a log-linear decrease in strain rate to 3×10^{-8} s^{-1} at 4% axial strain. At 75°C, the strain rate decreased to 10^{-8} s^{-1} within 1.5% axial strain from the onset of creep, with a just brief increase in strain rate by half an order of magnitude at 1.6% strain. A total of two stress steps were carried out during this 75°C test, at 2.6% and 3.4% axial strain. For the experiment carried out at 150°C the starting creep stress was 53 MPa, which was the lowest differential creep stress used in this study. At this stress level, it took a further 2% axial strain before the strain rate reached the lower limit of 10^{-8} s^{-1} and a stress step was performed.

5. Discussion

5.1. Summary of Key Observations

The single stress level creep tests (Figures 1 and 2) and the stress stepping creep test (Figure 3) show a few key qualitative trends. In general, the porosity reduction as a function of axial strain was similar between samples deformed under both CSR and constant stress conditions, which shows that the volumetric change of the sample is linked to the axial strain of the sample. This relationship does not appear to be measurably affected by strain rate. The Young's modulus of all of our experiments was between 6 and 11 GPa and showed no relationship with temperature, which is in concordance with the results of Jefferd et al. (2021). The variation in the Young's moduli is likely down to sample heterogeneity and small misalignment of the piston at lower stresses.

The creep experiments showed that in general, the axial strain rate decreased progressively with increasing strain under a constant differential stress. At all temperatures, the creep stress greatly influenced the creep strain rate.

More specifically, the rate of decrease in axial strain rate with increasing strain is greater at lower applied stress, that is the strain rate decays more rapidly at low stress than at high stress. For example, at room temperature, a creep stress of 93 MPa required 4% of axial strain past the onset of creep to reach a strain rate of 10^{-8} s^{-1}, whereas at a differential stress of 70 MPa only 1% of axial strain was required to reach a strain rate of 10^{-8} s^{-1}. At 150°C a differential stress of 78 MPa required 4.5% axial strain to slow to a strain rate of 10^{-8} s^{-1}, compared to 2% axial strain at a differential stress of 53 MPa.

The general trends in our experiments are very similar to those observed by Heap et al. (2015). In our highest creep stress ($Q = 93$ MPa) room temperature experiment the strain rate after 4% total axial strain was 1×10^{-7} s^{-1} compared to 8×10^{-8} s^{-1} at 4% total axial strain in the highest creep stress experiment ($Q = 92$ MPa) of Heap et al. (2015). The comparability of the data between the two studies is useful in deducing any possible deformation styles or mechanisms, as accurate post deformation visual inspection of our samples at the macro and micro scales was not possible due to sample alteration/destruction during removal from the apparatus or jacket deterioration caused by the long experiment duration and P/T conditions.

5.2. Comparison Between Constant Strain Rate and Creep Experiments

From a qualitative viewpoint, the continuous decrease in strain rate during creep is observed at the axial strains values where linear strain hardening is typically seen in CSR tests. Therefore, at a given amount of axial strain the creep experiments have experienced a "stress deficit" compared to the reference CSR test. Creep experiments on sandstone in the dilatant brittle regime, have demonstrated that the strain rate evolution throughout an experiment mirrors the difference in differential stress (ΔQ) between a creep experiment and a reference CSR experiment. Brantut et al. (2014) observed that the lowest strain rate during brittle creep (i.e., transition from primary to tertiary creep) occurred when the magnitude of ΔQ was largest. In our compactant creep experiments, the strain rate decreases continuously with increasing axial strain, which is analog to a continuous region of primary creep seen in the brittle regime. We can then use a similar approach employed by Brantut et al. (2014), where the difference in differential stress between the CSR and each creep experiment can be related to the strain rate ratio between the tests. The stress difference ΔQ taken between two samples undergoing different deformation histories makes physical sense only if it is taken at the same microstructural state of the samples (Brantut et al., 2014). Here, in absence of in situ direct measurements of the microstructure, we follow Brantut et al. (2014) and use the inelastic axial strain as a proxy for microstructural state. It is a reasonable choice since inelastic axial strain is the manifestation of microstructural changes, and naturally corrects for the variations in samples' static moduli. The inelastic strain (ϵ_{IE}) is calculated for the duration of the experiment $\epsilon_{IE} = \epsilon_{total} - Q/E$, where ($\epsilon_{total}$) is the total axial strain, and E is the Young's modulus. ΔQ is then calculated by subtracting the creep differential stress from the ever increasing CSR differential stress at a given inelastic strain.

For all experiments the strain rate at the onset of the first creep phase is equal to the imposed 10^{-5} s^{-1} of the CSR loading period. Following the start of the creep phase the strain rate decreases with time and increasing axial strain. The strain rate at both room temperature (Figure 4) and at 150°C (Figure 5) reduces as ΔQ becomes more negative. The strong dependence of the strain rate on ΔQ is clearest shortly after the start of the creep phase. At this point, the samples have only undergone minimal inelastic strain (<1%) and are therefore more likely to be in a similar microstructural state. Once more strain is accumulated and the microstructural state of each sample becomes more different from one another some slight discrepancies are observed. For example, the two experiments performed at creep stresses of 66 and 78 MPa and 150°C (Figure 5), had very similar strain rates from 2% to 4% inelastic strain, despite the difference in ΔQ being almost 15 MPa. The experiment performed at $Q = 66$ MPa experienced a slight strain rate increase of half an order of magnitude.

Occasionally during our experiments, the strain rate increased by up to an order of magnitude for a brief period, such as the experiment performed at $Q = 66$ MPa. In the study from Heap et al. (2015), compaction creep experiments were carried out on the comparable Bleurswiller sandstone and it was noted that periods of increased strain rate also occurred and these coincided with a surge in acoustic emission activity. Post-processing of the acoustic emissions showed that the bulk of the deformation occurring during these compactant events were located in localized sub-horizontal compaction bands. In our experiment, the periods of strain rate increase were generally observed during the creep experiments with lower differential stress, such as in Figures 2 and 3. The observed increase in strain rate occurred around 1.5% axial strain, which is approximately the same amount of strain as the rollover and plateau in the CSR experiments. The rollover and plateau is often associated with the

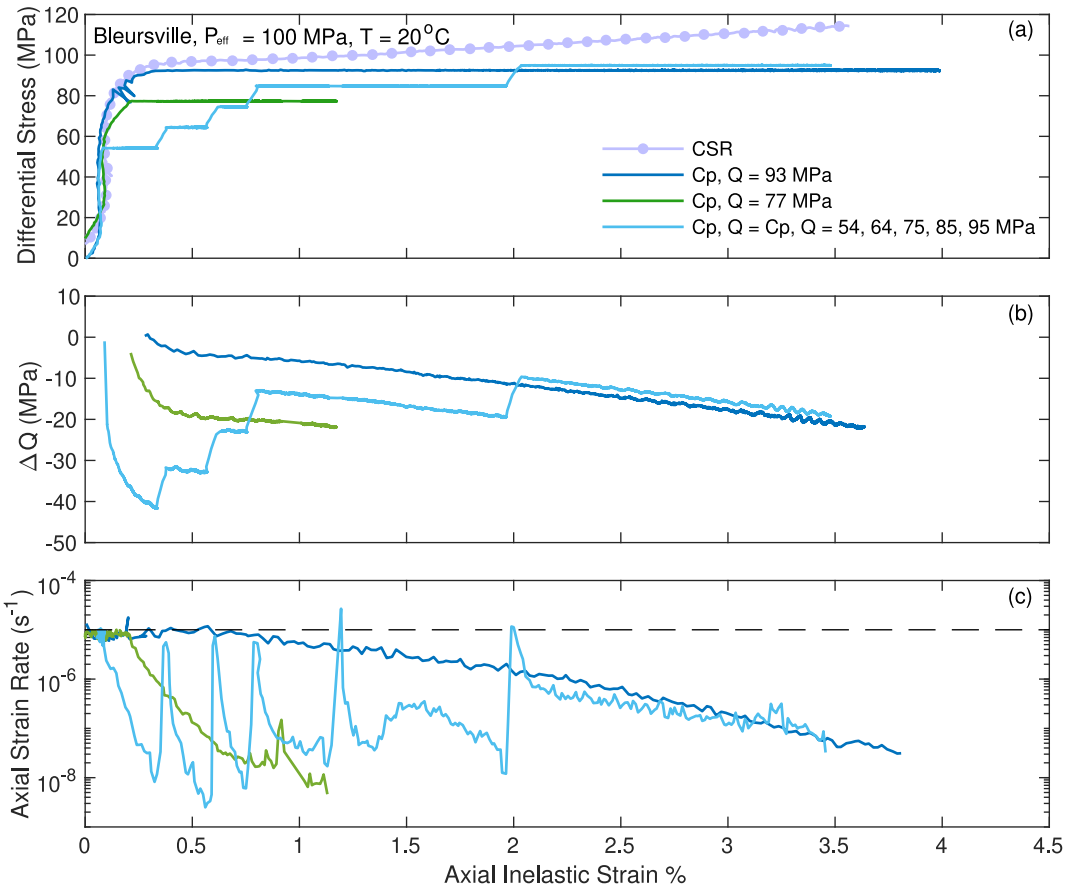

Figure 4. (a) Differential stress plotted against inelastic axial strain for a constant strain rate (CSR) test, marked CSR (dots) and three creep tests, marked Cp (lines), performed at room temperature. (b) The difference in differential stress between the creep tests and the CSR test as a function of inelastic axial strain. (c) Axial strain rate plotted as a function of inelastic strain for the creep experiments in (a). The black dashed line indicates a strain rate of 10^{-5} s^{-1} which is the strain rate of CSR experiments and the loading phase of the creep experiments.

weakening of the rock and moving away from strain hardening behavior due to the introduction of widespread damage (localized or diffused) in the sample. Jefferd et al. (2021) showed through microstructural imaging that when Bleursville sandstone was deformed to 5% strain under CSR conditions at the same P/T conditions used in this study, the areas of high damage and grain fracturing were not in discrete compaction bands, as seen in Heap et al. (2015) but in more diffusive bands throughout the sample. While we cannot be fully confident that the damage mechanism is the same in this study, the logic of Brantut et al. (2014), where axial strain was used as proxy for microstructural state of the sample implies that the increased periodic strain rates observed in this study also coincide with a compactant event and possibly the formation of diffusive compaction bands. Following a compactant event, it is possible that this caused a weakening of the rock (or part of the rock), which caused the observed higher strain rate following it.

5.3. "Activation Stress" of Ductile Creep

For each of the creep experiments it is generally observed that the strain rate decreases as ΔQ becomes more negative, regardless of the temperature used. However, the rate at which the strain rate decreases with a more negative ΔQ is affected by the temperature (Figure 6a), with the experiments conducted at elevated temperature displaying a slower decrease with a decreasing ΔQ. In previous work which looked at the brittle creep of sandstone, Brantut et al. (2014) established that the strain rate at a given value of ΔQ could be described by

$$\dot{\epsilon}_{creep} \approx \dot{\epsilon_0} \exp(\Delta Q/\sigma^*), \quad (1)$$

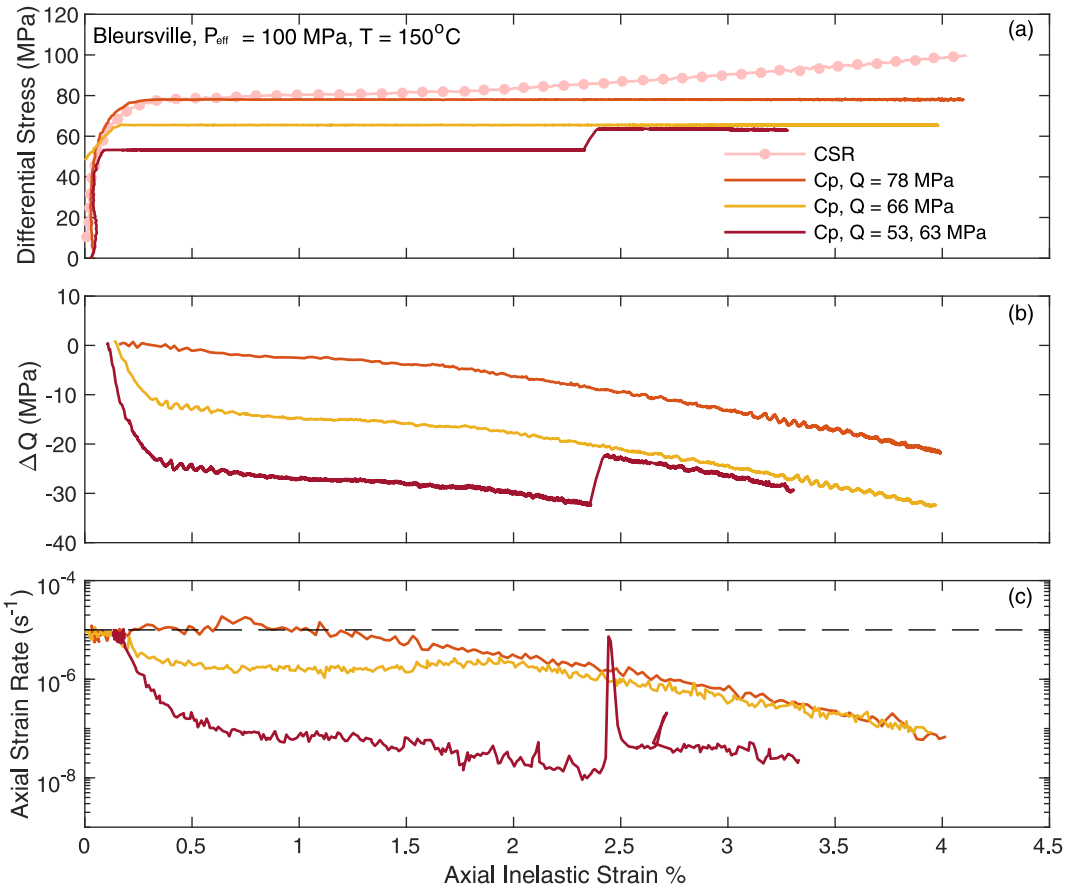

Figure 5. (a) Differential stress plotted against inelastic axial strain for a constant strain rate (CSR) test, marked CSR (dots) and three creep tests, marked Cp (lines), performed at 150°C. (b) The difference in differential stress between the creep tests and the CSR test as a function of inelastic axial strain. (c) Axial strain rate plotted as a function of inelastic strain for the creep experiments in (a). The black dashed line indicates a strain rate of 10^{-5} s^{-1} which is the strain rate of CSR experiments and the loading phase of the creep experiments.

where $\dot{\epsilon}_{creep}$ is the instantaneous strain rate during creep, $\dot{\epsilon}_0$ is the reference strain rate from the CSR experiment and σ^* is an activation stress, which determines the stress dependency on the observed strain rate.

The concept of the stress deficit and what it represents when comparing creep and CSR experiments is explicitly described by Brantut et al. (2014). However, in summary, the stress deficit corresponds to the difference in irrecoverable work (or input energy) required to achieve some unit of inelastic strain. In our "fast CSR" experiments the microstructural evidence presented in Jefferd et al. (2021) suggested that microfracturing and pore collapse facilitated macroscopic compaction of the samples. These processes are essentially brittle in nature and due to the short timescales involved are assumed to occur when the local stress intensity factor K_I reaches some critical value K_{IC}, which is determined by the fracture toughness of a mineral. The magnitude of K_I depends on the local grain geometry and the applied external macroscopic stress. As the differential stress is lower during the creep experiments than during the CSR experiments the average magnitude of K_I must also be lowered, which means that the stress deficit can also be thought of as a K_I deficit.

In our experiments, the strain rate reduction as ΔQ decreases appears to be relatively temperature insensitive when ΔQ is greater than approximately −10 MPa (Figure 6a). As ΔQ continues to becomes more negative the rate of strain rate decrease is less at elevated temperature and this is reflected in the activation stress becoming greater (activation stress is represented by the gradient of the curves in Figure 6a). Once ΔQ becomes less than −10 MPa the room temperature experiments have an activation stress of between 2.5 and 4 MPa, compared to values of between 4.5 and 5.5 MPa at 75°C, and 5 and 6 MPa at 150°C. The increasing activation stress with increasing temperature signifies that the stress sensitivity of the time-dependent deformation is lower at higher temperatures.

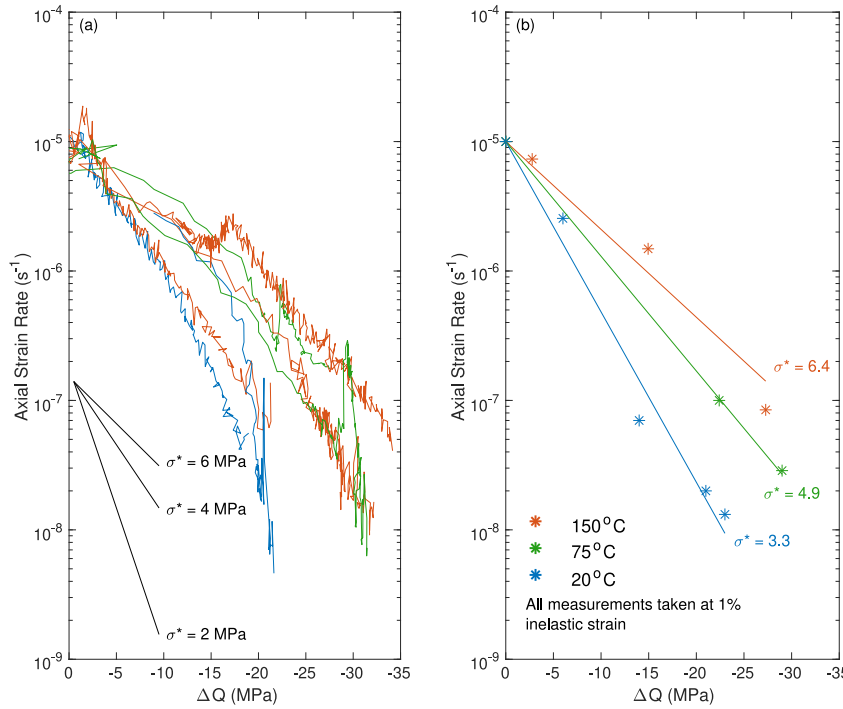

Figure 6. (a) The axial strain rate plotted as a function of increasing ΔQ for the duration of the experiments. The blue lines represent room temperature experiments, green line represent 75°C and red lines represent 150°C. (b) The markers indicate both the axial strain rate and ΔQ at 1% inelastic strain. The lines represent an empirical model and are calculated using Equation 1.

In the work by Heap et al. (2015), an activation stress of around 4 MPa was determined for compaction creep experiments performed on Bleurswiller sandstone at an effective pressure of 80 MPa and at room temperature.

From the strain rate curves (Figures 4 and 5) it is clear that not every sample followed the exact same evolution of strain rate with increasing axial inelastic strain, as some experiments underwent a notable compactant event(s) and some experiments did not. The variable evolution of strain rate with increasing axial strain between different samples indicates that the microstructural evolution varies between samples in different experiments. To assess how the strain rate evolves as a function of ΔQ when the samples are more microstructurally similar, the value of ΔQ and the strain rate can be measured at 1% inelastic strain for each experiment (Figure 6b). Assuming that at zero ΔQ the strain rate is 10^{-5} s^{-1}. An activation stress of 3.3 MPa at room temperature, 4.9 MPa at 75°C and 6.5 MPa at 150°C was measured (Figure 6b).

The difference in the activation stress at different temperatures implies that at higher temperatures the strain rate is less sensitive to an increase in ΔQ. Additionally, we observe that at lower values of ΔQ, the strain rate is less dependent on temperature than when ΔQ is larger (Figure 6b).

The trend of strain rate as a function of ΔQ (Equation 1) is useful for comparing the sensitivity of a change in stress to strain rate at a given temperature. These data can then be recast in terms of deformation rate versus absolute differential stress, if we assume that $\Delta Q = 0$ MPa corresponds to the reference strain rate of 10^{-5} s^{-1} (Figure 7). From the CSR tests, the differential stress required for a strain rate of 10^{-5} s^{-1} at 1% inelastic strain is 100 MPa at room temperature and 80 MPa at 150°C, reflecting a 20 MPa reduction. In contrast, at a strain rate of 10^{-7} s^{-1}, the differential stress required is 85 MPa at room temperature and 53 MPa at 150°C, which is a difference of 32 MPa. At the intermediate temperature of 75°C, the stress difference to the room temperature test changes from 11 MPa at 10^{-5} s^{-1} to 19 MPa at 10^{-7} s^{-1}, showing that even a modest temperature increase of 55°C is enough to both weaken the rock in the short duration CSR experiments and also to alter the time-dependent behavior in the longer duration creep experiments. The larger stress differences observed at the lower strain rates indicate that elevated temperature has a more pronounced weakening effect at lower deformation rates.

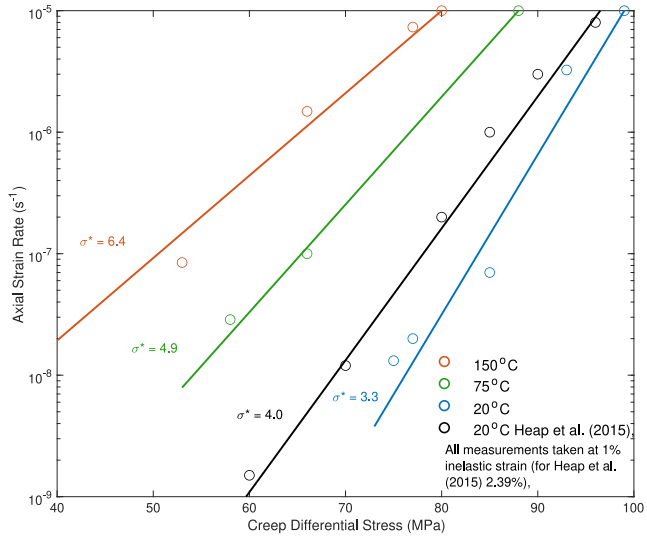

Figure 7. The markers show the axial strain rate and differential stress at 1% inelastic strain. The lines represent an empirical model, and are calculated using Equation 1. Included in black is the room temperature data from Heap et al. (2015).

The temperature dependency of the activation stress can be understood by considering the creep law (Equation 1) as the macroscopic manifestation of thermally activated rate process. In that framework, the activation stress can be written as

$$\sigma^* \approx C \times RT/V^*, \tag{2}$$

where R is the ideal gas constant, T is the absolute temperature, V^* is an activation volume and C is a numerical factor accounting for the geometry and statistics of the volume elements undergoing thermally activated deformation (e.g., microcracks in the context of subcritical crack growth, see Brantut et al. (2014)). The activation stress extracted from our data set seems to be proportional to temperature (Figure 8), with a mean factor V^*/C of 6.0×10^{-4} m^3/mol (with a range of 5.5–7.4 $\times 10^{-4}$ m^3/mol). This value is 6–20 times larger than the molar volume of plagioclase feldspar and quartz, respectively, assuming C is of order unity or smaller. In the brittle regime, Brantut et al. (2014) derived an explicit expression for the factor C for a wing-crack like model, but it is not fully clear whether that expression applies in the ductile regime, where grain crushing is likely more dominant. That being said, Equation 17 of Brantut et al. (2014) suggests that C may be on the order of 0.01, i.e., much less than 1. If C is indeed significantly smaller than 1, then the corresponding activation volume V^* would be

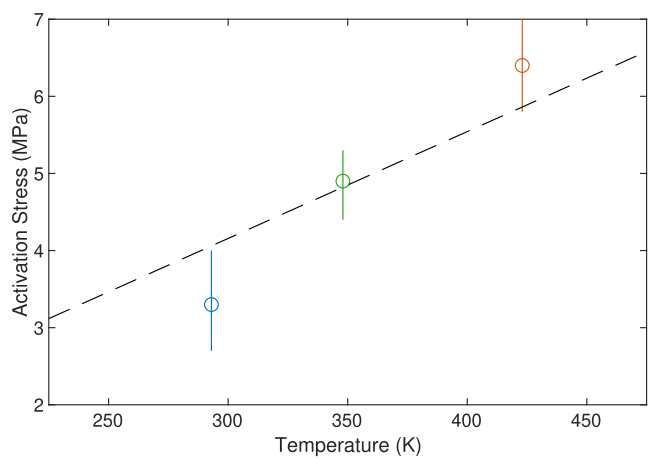

Figure 8. The calculated activation stress from our experiments as a function of temperature. A line is added using the relationship shown in Equation 2 and a V^*/C value of 6.0 $\times 10^{-4}$ m^3/mol.

comparable to the molar volumes of the mineral constituents of the rock. This would imply that the rate-limiting step in the creep process operates on a scale incorporating a few molecules.

The degree of approximation made in the determination of activation stress, and the semi-empirical nature of the creep law (Equation 1) limits our ability to draw any strong conclusions regarding the deeper meaning of the activation volume. Despite these limitations, our simple approach provides a consistent explanation for the change in stress dependency at increasing temperature, and is consistent with more mechanistic models established in the context of creep in the brittle regime driven by subcritical crack growth (Brantut et al., 2014).

5.4. Possible Temperature Sensitive Time-Dependent Micro-Mechanical Mechanisms

The creep experiments have demonstrated that sandstone deformation in the ductile regime exhibits a time dependency in the temperature range of 20 to 150°C. The results show that the effect of elevated temperature on time-dependent deformation in the ductile regime appears to be twofold. Firstly, at a given differential stress the observed strain rate is higher at 150°C than at room temperature and secondly, the stress sensitivity of the decreasing strain rate with increasing axial strain is reduced.

Several micro-mechanical mechanisms have been proposed to explain the development of inelastic sandstone compaction under both laboratory conditions and in natural environments. For sandstones with a mixed mineralogy and containing small amounts of clay, such as the Bleursville sandstone used in this study, triaxial deformation experiments have indicated that the deformation of grain boundaries and intergranular sliding is likely the dominant inelastic deformation mechanism at smaller axial strains (<0.5%) (Bernabe et al., 1994; David et al., 2001; Menéndez et al., 1996; Pijnenburg et al., 2018, 2019a). At higher axial strains (>0.5%), the primary inelastic deformation mechanism likely transitions to intragranular cracking and cataclastic flow (Baud et al., 2000; Bernabe et al., 1994; Heap et al., 2015; Menéndez et al., 1996; Wong et al., 1997). Typically, the onset of widespread intragranular fracturing is observed as the stress-strain relationship deviates away from linearity, which is often at approximately 0.5%–1% axial strain (Menéndez et al., 1996; Wong & Baud, 1999).

Under an effective pressure of 100 MPa Bleursville sandstone has a macroscopic yield point (C^*) at approximately $Q = 63$ MPa at room temperature and $Q = 48$ MPa at 150°C (Jefferd et al., 2021). All but one of the creep stresses used was higher than the respective yield stress and when the creep stress was below the yield stress, only minimal additional inelastic strain was detectable (Figure 3).

The deformation of grain boundary structures and potentially any clay deposited there could contribute to the deformation in the early stages of our experiments. The average grain size of Bleursville sandstone is approximately 100 microns, but the undeformed grain boundary thickness is of the order of a few microns (Jefferd et al., 2021; Pijnenburg et al., 2019b). Therefore even if the entire grain boundary thickness was to be removed, the total strain would not be able to reach much above 1% total strain. Furthermore, Pijnenburg et al. (2019b) theoretically established that the thin nature of grain boundaries means that the compaction of the grain boundaries, which is caused by the release of fluids from the internal clay structures, is likely instantaneous on the time scale of these experiments. Clay deformation in the grain boundaries is therefore not likely to contribute much to the inelastic strain occurring after 0.5% strain or in any of the time-dependent deformation.

Our experiments indicate that the weakening at elevated temperature is enhanced at lower strain rates. This effect could originate from thermally activated rate-dependent friction between grain contacts. There is experimental evidence that gouge material produced from Scholteren sandstone, (a sandstone compositionally akin to Bleursville sandstone) exhibits velocity-strengthening behavior, that is the friction coefficient is lower at slower sliding velocities, in a ring-shear set-up (Arts et al., 2024; Hunfeld et al., 2017). Hunfeld et al. (2017) observed that an increase in sliding velocity of 2 orders of magnitude resulted in an increase in friction coefficient from 0.58 to 0.62. Uncertainties remain however about how friction data produced on gouge in a ring shear set-up can be applied to compaction in the bulk granular sandstone. There is also currently no known experimental data which has systematically assessed the role of temperature on the velocity-strengthening observed, making it difficult to conclude how internal friction may play a role in our experiments.

As mentioned previously, subcritical crack growth could be the dominant deformation mechanism producing time-dependent compaction creep in the conditions of our experiments. The accumulation of inelastic strain through microcracking requires both of the serial operating processes of microcrack generation and growth, and sliding on the newly formed microcracks. If we assume that the frictionally controlled sliding on the microcrack is

not the rate controlling process and the microcrack formation is, we can say that the strain rate when grain fracturing is involved is essentially the macroscopic manifestation of the microcrack growth velocities. As described by Atkinson and Meredith (1981), subcritical cracking produces crack growth rates several orders of magnitude lower than those generated by cracking at critical conditions. Therefore, at lower strain rates, where on average the microcrack growth rate is slower, the contribution of subcritical cracking is expected to be larger.

The temperature dependence of the creep compaction rate, as described by the semi-empirical Equation 1 and a temperature-dependent activation stress (Figure 8, Equation 2), is consistent with subcritical crack growth. Double torsion experiments have shown that crack growth velocity is increased in quartzites (Atkinson, 1980) and in sandstones containing other minerals including feldspars and clays (Nara et al., 2011). The work of Nara et al. (2011) established that for the feldspar and clay rich Shirahama sandstone a temperature increase of a modest 30°C was sufficient to increase crack growth velocities by almost an order of magnitude. At lower effective pressures under which sandstone deforms in a more macroscopically brittle manner, Heap, Baud, and Meredith (2009) demonstrated using triaxial deformation experiments on three different sandstones that (a) a direct weakening effect was observed when the deformation temperature was increased from room temperature to 75°C at identical strain rates and that (b) the stress sensitivity on strain rate during stress stepping brittle creep experiments was reduced. Both points are similar to what we observed in our experiments.

From a theoretical point of view, the two-fold effect of temperature on creep rate is also consistent with established subcritical cracking models. For instance, as described by Wiederhorn (1974), the crack growth rate (ν) due to subcritical cracking facilitated by stress corrosion, follows the form,

$$\nu = \nu_0 \exp\left[-\frac{\Delta H + 2V^* K_I/\sqrt{\pi\rho}}{RT}\right], \tag{3}$$

where ν_0 is a pre-exponential factor, ΔH is an activation enthalpy, R is the gas constant, T is the absolute temperature, K_I is the stress intensity factor, V^* is an activation volume and ρ the radius of the crack tip. Increasing the temperature impacts crack velocity via both the activation enthalpy, which provides a direct increase in ν, and via the activation volume, which reduces the K_I sensitivity and thus the stress sensitivity of ν. These effects are qualitatively similar to our results and our semi-empirical creep law (Figure 7), and are in line with previous results obtained in the brittle creep regime (Brantut et al., 2014). Equation 3 also highlights how an increase in the stress deficit (ΔQ) corresponds to a decrease in the strain rate. At a given microstructural state, the cracks with the lowest K_I deficit will continue to grow the fastest. After the "easy" cracks break, the remaining cracks have a greater K_I deficit and will grow slower, which corresponds to a lower strain rate.

An additional deformation process which could lead to the time-dependent compaction observed in our experiments is intergranular pressure solution. Deformation via pressure solution is driven by the dissolution of material at highly stressed grain interfaces followed by the diffusion of the material through pore wall fluid films and finally the precipitation of material at lower stressed grain boundaries (e.g., Niemeijer et al., 2002; Rutter, 1976). The rate of deformation associated with pressure solution results from the slowest operating process out of; dissolution, diffusion and precipitation, and in a pure quartz system the rate controlling process is likely the rate of dissolution (Renard et al., 2000). It is anticipated that at depths greater than 5 km in the crust, intergranular pressure solution may well be the dominant driving force of time-dependent deformation (Niemeijer et al., 2002; Rutter, 1976; Spiers et al., 2003). Pressure solution is known to have a temperature dependence and 150°C is regularly assumed to be toward the lower bound temperature of detectability in quartz rich rocks (e.g., Niemeijer et al., 2002; Rutter, 1976). Various attempts have been made to establish kinetic based models for the rate of pressure solution and by using the model of Pluymakers and Spiers (2015), we can calculate an estimated strain rate of diffusion controlled pressure solution ($\dot{\epsilon}_{ps}$) for a quartz based system of imperfectly packed, granular aggregate, which is given by

$$\dot{\epsilon_{ps}} = \frac{A_s}{d} I_s \left[\exp\left(\frac{\sigma_n^e \Omega}{RT}\frac{Z}{F}\frac{q}{q-2\phi}\right) - 1\right], \tag{4}$$

where A_s is a geometric factor and is equal to 6 for 3D isotropic compaction and 2 for 1D compaction (Pluymakers & Spiers, 2015), d is the mean grain size, σ_n^e is the effective macroscopic normal stress and can therefore be given

by $\sigma_1 - P_p$, Ω is the molar volume of quartz, R is the gas constant, T is the absolute temperature, Z is the grain coordination number and can be equated to 6 for a cubic system (X. Zhang et al., 2010), F is the grain shape factor and can be equated to π for spherical grains (Pluymakers & Spiers, 2015), q is a geometric term that equals double the maximum porosity of a pack of regular spherical grains at the point where the grains are just touching (i.e., 0.8 to 0.1) (Pluymakers & Spiers, 2015), ϕ is the porosity, and I_s is the dissolution rate constant and can be given by $\alpha k_+ \Omega$. α corresponds to a grain boundary shape factor and can be assumed to equal 0.9 (van Noort et al., 2008). k_+ is the geochemical dissolution rate constant for the unstressed solid, which for quartz has a value of 0.1–1 $\times 10^{-5}$ mol m^{-2} s^{-1} at 150°C (R. Zhang et al., 2015). Using Equation 4, the strain rate for a pure quartz system with a grain size of 120 microns is likely on the order of high 10^{-10} s^{-1} and 10^{-13} s^{-1} at 150°C and 20°C, respectively.

When using Equation 4 to calculate the strain rate due to pressure solution we assume that there is no minimum temperature at which pressure solution can occur. We also neglect the possible existence of a minimum threshold stress below which the rate of pressure solution is zero (van Noort et al., 2008). We also acknowledge that the rate of pressure solution calculated for a pure quartz based system may be lower than in a polymineralic system with quartz, feldspar and clays present. The dissolution, diffusion and precipitation rate of quartz may be locally increased by 2 orders of magnitude if clay or mica is present next to quartz in the grain boundary (Gundersen et al., 2002; Oelkers et al., 2000; Renard et al., 1997). In any case, the deformation rate from pressure solution is typically lower than the lowest rate achieved in our experiments, making this process unlikely to play a significant role in the conditions tested.

5.5. Extrapolation to Low Stress States

Our laboratory results can be extrapolated to longer time-scales by combining the two existing creep laws (from subcritical cracking and pressure solution) into a composite creep law. In a system where two or more independent deformation processes are operating in parallel to one another, the macroscopic strain rate is controlled by the fastest deformation mechanism. To determine under what conditions subcritical cracking or pressure solution might be the rate-controlling deformation process, we constructed a composite creep law based on the applied stress and the grain size of the material, summing the contribution of each deformation mechanism to compute the total strain rate. The strain rate expected solely from pressure solution is calculated from Equation 4 and the strain rate expected as a result of stress corrosion cracking is calculated by inserting the obtained values of the activation stresses shown in Figure 7 into Equation 1, which translates to

$$\dot{\epsilon} = 1 \times 10^{-5} \exp\left(\frac{Q - 99}{3.3}\right), \tag{5}$$

at room temperature and

$$\dot{\epsilon} = 1 \times 10^{-5} \exp\left(\frac{Q - 80}{6.5}\right), \tag{6}$$

at 150°C.

The total strain rate predicted at both temperatures is dominated by the subcritical cracking process at high stress, and switches gradually to pressure-solution at lower stress (Figure 9). At 150°C, our simple extrapolation of the subcritical cracking creep law implies that pressure solution should not be dominant even at stresses as low as a few 10s of MPa. At ambient temperature, the switch to pressure-solution is anticipated at strain rates of the order of 10^{-13}/s, which reinforces the above conclusion that pressure solution is unlikely to be playing a role in the deformation of Bleursville sandstone even at the lowest strain rates reached in our experiments.

A further factor to consider with the interpretation of the predicted strain rates in Figure 9 is that the strain rates calculated using Equations 4–6 only represent the strain rates at a specific chosen microstructural condition, which we simplify as given by a constant strain. The calculations for the rate of subcritical cracking were based on the stress strain rate relationship at 1% axial inelastic strain and therefore do not capture the decrease in strain rate due to the increasing difficulty of producing cracks and crushing grains as strain increases. However, the activation stresses obtained in Figure 6a were comparable to those obtained at 1% strain in Figure 6b. It is therefore

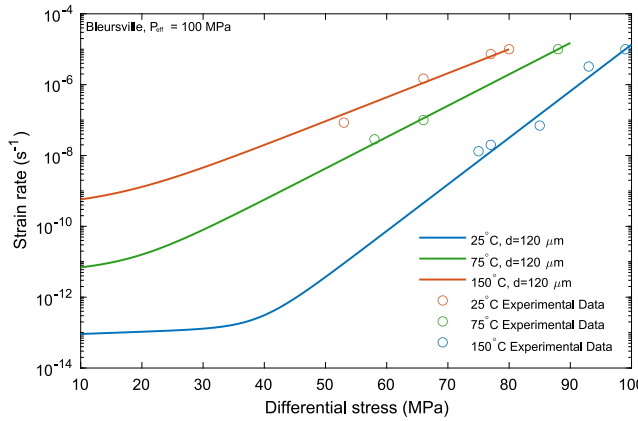

Figure 9. An extrapolation of the empirical creep rates obtained in the laboratory combined with the calculated pressure solution rates for Bleursville sandstone at an effective pressure of 100 MPa. At a temperature of 20°C (blue), 75°C (green) or 150°C (red). Included in circles is the measured strain rate at 1% axial inelastic strain from the experiments.

probable that they should hold true for at least a few percent strain. Likewise, the stress amplification factor (B) and the grain packing factor (f) in Equation 4 will also decrease with strain, leading to a reduction in the pressure solution strain rate.

While our extrapolations have suggested that at the temperature and pressure ranges used in our experiments, pressure solution is not a dominant driving source of deformation, one important aspect that has not been explicitly considered is grain size. Equation 3 demonstrates that the rate of subcritical crack growth is determined by the local stress intensity factor K_I and is therefore affected by the macroscopic applied stress, the grain size and grain shape. Additionally, the rate of pressure solution is known to be highly grain size dependent. For example, reducing the grain size in 4 by a factor of 10 to 12 microns increases the calculated pressure solution rate from high 10^{-10} s^{-1} to mid 10^{-9} s^{-1}. While the grain size of Bleursville sandstone is fairly regular at about 100–120 microns, there are some much smaller grains present (Jefferd et al., 2021). It is therefore possible that some of the smaller grains may be deforming via pressure solution while the larger grains deform via stress corrosion cracking. However, in the absence of a more complete creep law for subcritical cracking that would include grain size, composition and porosity, it is difficult to fully extrapolate our simple stress corrosion model to very low stresses and strain rates or to sandstones of different microstructural characteristics. Overall, the extrapolation indicates a dominance of subcritical cracking processes at elevated temperature, but this is subject to caution since the empirical relationship (1) has only experimental support for low stress deficits (a few tens of MPa).

5.6. Implications for Crustal Deformation Processes

Crustal strain rates involving sandstone deformation can cover many orders of magnitude. For example, the generation of compactant deformation bands in fault damage zones during dynamic seismic events may occur in under a second (Aben et al., 2017), whereas anthropogenic induced compaction of reservoir rocks through hydrocarbon extraction typically operates over decadal time-scales. In turn, however, this human induced compaction is still many orders of magnitude faster than natural diagenesis or tectonic loading (Mazzotti & Gueydan, 2018).

The extrapolations of the empirical creep rates obtained in the laboratory combined with theoretical pressure solution laws suggest that at typical crustal strain rates of 10^{-13} s^{-1} to 10^{-14} s^{-1} it would appear that the dominant long term deformation mechanism would be pressure solution at an effective pressure of 100 MPa and a temperature of 150°C. However, when crustal deformation occurs at higher strain rates, such as after a seismic event or during the depletion of reservoirs, it is possible that deformation may be caused by subcritical cracking. Deformation bands or compaction bands are often thought to occur in the compactant quadrant of a damage zone surrounding a fault (Fossen et al., 2007; Torabi et al., 2021). From micostructural analysis (Aben et al., 2017; Bésuelle & Rudnicki, 2004) it is clear that the formation of deformation bands involves the fracturing and breaking of grains, something which cannot be facilitated by pressure solution. As subcritical cracking can lead to

the fracturing of grains in the compactant regime (Heap et al., 2015) it is possible that deformation bands can be formed or at least grow in a time-dependent manner and are therefore sensitive to temperature.

Many instances of sandstone compaction which are of importance to humans occur as a result of hydrocarbon extraction and geo-storage practices. Typically, the depths of the hydrocarbon reservoirs is around 2–4 km where the effective pressures and temperatures are lower than in this study (Pijnenburg et al., 2018). The operational duration of a reservoir is also much shorter than typical geological timescales and therefore the measured compactant strain rates can be of the order of 10^{-11} s^{-1} to 10^{-12} s^{-1} (e.g., NAM (2016)). A reduction in depth, and therefore temperature, has been shown to suppress pressure solution more than subcritical cracking, therefore, it is possible that in certain reservoir settings, subcritical cracking may play a role in generating inelastic compaction. It is also recognized that all of our experiments were performed with water as the pore fluid, whereas in the crust, both the natural and human introduced fluids will have greatly different chemical properties and pH; and therefore may impact stress corrosion cracking and pressure solution differently.

The work by Jefferd et al. (2021), demonstrated that an elevated temperature of 150°C weakens sandstones even over short term time-scales. Here, we have shown that over longer timescales, the effect of elevated temperature becomes even more pronounced as time-dependent deformation mechanisms start to play a role. The two main observations are that (a) at higher temperatures the stress level required for any (measurable) inelastic time-dependent deformation is lowered, and that (b) the stress dependence on time-dependent deformation is reduced at higher temperatures. It is therefore important that any models which take into account inelastic sandstone deformation over long periods of time include the effect of temperature when calculating the expected strain rates due to time-dependent processes.

6. Conclusions

We presented results from a series of compactant creep experiments performed at either room temperature, 75°C or 150°C at a constant effective pressure of 100 MPa on Bleursville sandstone. Different values of differential stress were used in each experiment to establish the stress sensitivity of creep at each tested temperature. In all conditions, experiments showed a decreasing axial strain rate with axial strain increased. At differential stresses between 55 and 75 MPa, the experiments performed at 75°C or 150°C continued to creep at detectable levels, whereas at room temperature, strain rates fell below the measurable limit of 10^{-8} s^{-1}. At any given differential stress, creep rates were faster at elevated temperatures (75°C or 150°C) than at room temperature. In addition, the stress sensitivity of creep decreased with increasing temperature, as measured by an increase in the empirically derived "activation stress" from 3.3 MPa at room temperature to 4.9 MPa at 75°C and 6.5 MPa at 150°C. The change in stress sensitivity of creep with increasing temperature can be interpreted in terms of an activation volume for the creep process, which is found to be commensurate with the molecular volume of the mineral constituents of the tested rock. The overall phenomenology of creep in the compactant, ductile regime is consistent with a mechanism driven by subcritical crack growth. In particular, the increased strain rate at higher temperatures can be attributed to an increase in subcritical crack growth velocities, which is in line with previous experimental work in the brittle creep regime. By comparing the derived empirical relationship of subcritical cracking with theoretical models of pressure solution it was concluded that pressure solution likely controls the rate of sandstone compaction over long geological timescales (at strain rates of 10^{-9} s^{-1} or below), the rate of subcritical cracking is likely sufficient to influence crustal deformation or reservoir mechanics at intermediate strain rates (10^{-9} s^{-1} and above). The rates of subcritical cracking were observed to have a temperature dependency and should be integrated into future models examining sandstone compaction and deformation under varying thermal conditions.

Conflict of Interest

The authors declare no conflicts of interest relevant to this study.

Data Availability Statement

The data related to this paper may be found at (Jefferd et al., 2025).

Acknowledgments
Financial support was received from the UK Natural Environment Research Council (grant NE/L002485/1) NB acknowledges support from the European Research Council under the European Union's Horizon 2020 research and innovation programme (project RockDeaf, grant agreement Number 804685). Discussions with Patrick Baud helped to shape this project. MJ thanks Chris Spiers and Suzanne Hangx for their fruitful discussions on pressure solution. Neil Hughes contributed to the design and construction of the triaxial apparatus. We also thank Teng-fong Wong and an anonymous reviewer who greatly improved this manuscript with their feedback.

References

Aben, F., Doan, M.-L., Gratier, J.-P., & Renard, F. (2017). High strain rate deformation of porous sandstone and the asymmetry of earthquake damage in shallow fault zones. *Earth and Planetary Science Letters*, *463*, 81–91. https://doi.org/10.1016/j.epsl.2017.01.016

Anderson, O. L., & Grew, P. C. (1977). Stress corrosion theory of crack propagation with applications to geophysics. *Reviews of Geophysics and Space Physics*, *15*(1), 77–104. https://doi.org/10.1029/rg015i001p00077

Arts, J. P., Niemeijer, A. R., Drury, M. R., Willingshofer, E., & Matenco, L. C. (2024). The frictional strength and stability of spatially heterogeneous fault gouges. *Earth and Planetary Science Letters*, *628*, 118586. https://doi.org/10.1016/j.epsl.2024.118586

Atkinson, B. K. (1980). Stress corrosion and the rate-dependent tensile failure of a fine-grained quartz rock. *Tectonophysics*, *65*(3–4), 281–290. https://doi.org/10.1016/0040-1951(80)90078-5

Atkinson, B. K., & Meredith, P. G. (1981). Stress corrosion cracking of quartz: A note on the influence of chemical environment. *Tectonophysics*, *77*(1–2), T1–T11. https://doi.org/10.1016/0040-1951(81)90157-8

Atkinson, B. K., & Meredith, P. G. (1987). 4 - The theory of subcritical crack growth with applications to minerals and rocks. In *Fracture mechanics of rock* (pp. 111–166). Academic Press. Retrieved 2016-02-23, from Retrieved from http://www.sciencedirect.com/science/article/pii/B9780120662661500090

Baud, P., Reuschlé, T., Ji, Y., Cheung, C. S., & Wong, T.-F. (2015). Mechanical compaction and strain localization in Bleurswiller sandstone. *Journal of Geophysical Research*, *120*, 6501–6522.

Baud, P., Schubnel, A., & Wong, T.-F. (2000). Dilatancy, compaction, and failure mode in Solnhofen limestone. *Journal of Geophysical Research*, *105*(B8), 19289–19303. https://doi.org/10.1029/2000jb900133

Bernabe, Y., Fryer, D., & Shively, R. (1994). Experimental observations of the elastic and inelastic behaviour of porous sandstones. *Geophysical Journal International*, *117*(2), 403–418. https://doi.org/10.1111/j.1365-246x.1994.tb03940.x

Bésuelle, P., & Rudnicki, J. W. (2004). Localization: Shear bands and compaction bands. In *International geophysics* (Vol. 89, pp. 219–321). Elsevier.

Brantut, N., Heap, M., Meredith, P., & Baud, P. (2013). Time-dependent cracking and brittle creep in crustal rocks: A review. *Journal of Structural Geology*, *52*, 17–43. https://doi.org/10.1016/j.jsg.2013.03.007

Brantut, N., Heap, M. J., Baud, P., & Meredith, P. G. (2014). Rate- and strain-dependent brittle deformation of rocks. *Journal of Geophysical Research*, *119*(3), 1818–1836. https://doi.org/10.1002/2013JB010448

David, C., Menendez, B., Zhu, W., & Wong, T. (2001). Mechanical compaction, microstructures and permeability evolution in sandstones. *Physics and Chemistry of the Earth - Part A: Solid Earth and Geodesy*, *26*(1–2), 45–51. https://doi.org/10.1016/s1464-1895(01)00021-7

Dewers, T., & Hajash, A. (1995). Rate laws for water-assisted compaction and stress-induced water-rock interaction in sandstones. *Journal of Geophysical Research*, *100*(B7), 13093–13112. https://doi.org/10.1029/95jb00912

Fortin, J., Schubnel, A., & Guéguen, Y. (2005). Elastic wave velocities and permeability evolution during compaction of bleurswiller sandstone. *International Journal of Rock Mechanics and Mining Sciences*, *42*(7–8), 873–889.

Fossen, H., Schulz, R. A., Shipton, Z. K., & Mair, K. (2007). Deformation bands in sandstone: A review. *Journal of the Geological Society*, *164*(4), 755–769.

Fredrich, J. T., Deitrick, G., Arguello Jr, J. G., & DeRouffignac, E. (2000). *Geomechanical modeling of reservoir compaction, surface subsidence, and casing damage at the belridge diatomite field (Tech. Rep.)*. Sandia National Labs.

Geertsma, J. (1973). Land subsidence above compacting oil and gas reservoirs. *Journal of Petroleum Technology*, *25*(6), 734–744. https://doi.org/10.2118/3730-pa

Gratier, J.-P., Renard, F., & Labaume, P. (1999). How pressure solution creep and fracturing processes interact in the upper crust to make it behave in both a brittle and viscous manner. *Journal of Structural Geology*, *21*(8–9), 1189–1197. https://doi.org/10.1016/s0191-8141(99)00035-8

Gundersen, E., Dysthe, D., Renard, F., Bjørlykke, K., & Jamtveit, B. (2002). Numerical modelling of pressure solution in sandstone, rate-limiting processes and the effect of clays. *Geological Society, London, Special Publications*, *200*(1), 41–60. https://doi.org/10.1144/gsl.sp.2001.200.01.03

Heap, M. J., Baud, P., & Meredith, P. G. (2009). Influence of temperature on brittle creep in sandstones. *Geophysical Research Letters*, *36*(19), L19305. https://doi.org/10.1029/2009GL039373

Heap, M. J., Baud, P., Meredith, P. G., Bell, A. F., & Main, I. G. (2009). Time-dependent brittle creep in Darley Dale sandstone. *Journal of Geophysical Research*, *114*(B7), B07203. https://doi.org/10.1029/2008JB006212

Heap, M. J., Brantut, N., Baud, P., & Meredith, P. G. (2015). Time-dependent compaction band formation in sandstone. *Journal of Geophysical Research*, *120*(7), 4808–4830. https://doi.org/10.1002/2015JB012022

Hunfeld, L., Niemeijer, A., & Spiers, C. (2017). Frictional properties of simulated fault gouges from the seismogenic groningen gas field under in situ p–t-chemical conditions. *Journal of Geophysical Research: Solid Earth*, *122*(11), 8969–8989. https://doi.org/10.1002/2017jb014876

Jefferd, M., Brantut, N., Meredith, P. G., & Mitchell, T. M. (2025). Raw mechanical and processed data for bleursville sandstone deformed under triaxial conditions, at different temperatures and timescales. [Dataset]. *NERC EDS National Geoscience Data Centre*. https://doi.org/10.5285/164834e4-efda-44c7-9bd2-aa0641482227

Jefferd, M., Brantut, N., Meredith, P. G., Mitchell, T. M., & Plümper, O. (2021). Compactive deformation of sandstone under crustal pressure and temperature conditions. *Journal of Geophysical Research: Solid Earth*, *126*(4), e2020JB020202. https://doi.org/10.1029/2020jb020202

Jiang, Q., Qi, Y., Wang, Z., & Zhou, C. (2013). An extended nishihara model for the description of three stages of sandstone creep. *Geophysical Journal International*, *193*(2), 841–854. https://doi.org/10.1093/gji/ggt028

Lawn, B. R. (1993). *Fracture of brittle solids* (2nd ed.). Cambridge University Press.

Martin, J., & Serdengecti, S. (1984). Subsidence over oil and gas fields. *Man-induced Land Subsidence*, *6*, 23–34. https://doi.org/10.1130/reg6-p23

Mazzotti, S., & Gueydan, F. (2018). Control of tectonic inheritance on continental intraplate strain rate and seismicity. *Tectonophysics*, *746*, 602–610. https://doi.org/10.1016/j.tecto.2017.12.014

Menéndez, B., Zhu, W., & Wong, T.-F. (1996). Micromechanics of brittle faulting and cataclastic flow in Brea sandstone. *Journal of Structural Geology*, *18*(1), 1–16.

NAM. (2016). Technical addendum to the winningsplan groningen 2016.

Nara, Y., Morimoto, K., Yoneda, T., Hiroyoshi, N., & Kaneko, K. (2011). Effects of humidity and temperature on subcritical crack growth in sandstone. *International Journal of Solids and Structures*, *48*(7–8), 1130–1140. https://doi.org/10.1016/j.ijsolstr.2010.12.019

Ngwenya, B. T., Main, I. G., Elphick, S. C., Crawford, B. R., & Smart, B. G. (2001). A constitutive law for low-temperature creep of water-saturated sandstones. *Journal of Geophysical Research*, *106*(B10), 21811–21826. https://doi.org/10.1029/2001jb000403

Niemeijer, A. R., Spiers, C. J., & Bos, B. (2002). Compaction creep of quartz sand at 400–600°c: Experimental evidence for dissolution-controlled pressure solution. *Earth and Planetary Science Letters*, *195*(3–4), 261–275. https://doi.org/10.1016/s0012-821x(01)00593-3

Oelkers, E. H., Bjørkum, P. A., Walderhaug, O., Nadeau, P. H., & Murphy, W. M. (2000). Making diagenesis obey thermodynamics and kinetics: The case of quartz cementation in sandstones from offshore mid-norway. *Applied Geochemistry*, *15*(3), 295–309. https://doi.org/10.1016/s0883-2927(99)00047-5

Pijnenburg, R., Verberne, B., Hangx, S., & Spiers, C. (2018). Deformation behavior of sandstones from the seismogenic groningen gas field: Role of inelastic versus elastic mechanisms. *Journal of Geophysical Research: Solid Earth*, *123*(7), 5532–5558. https://doi.org/10.1029/2018jb015673

Pijnenburg, R., Verberne, B., Hangx, S., & Spiers, C. (2019a). Inelastic deformation of the slochteren sandstone: Stress-strain relations and implications for induced seismicity in the groningen gas field. *Journal of Geophysical Research: Solid Earth*, *124*(5), 5254–5282. https://doi.org/10.1029/2019jb017366

Pijnenburg, R., Verberne, B., Hangx, S., & Spiers, C. (2019b). Intergranular clay films control inelastic deformation in the groningen gas reservoir: Evidence from split-cylinder deformation tests. *Journal of Geophysical Research: Solid Earth*, *124*(12), 12679–12702. https://doi.org/10.1029/2019jb018702

Pluymakers, A. M., & Spiers, C. J. (2015). Compaction creep of simulated anhydrite fault gouge by pressure solution: Theory v. experiments and implications for fault sealing. *Geological Society, London, Special Publications*, *409*(1), 107–124. https://doi.org/10.1144/sp409.6

Renard, F., Brosse, E., & Gratier, J. (2000). The different processes involved in the mechanism of pressure solution in quartz-rich rocks and their interactions. *Quartz Cementation in Sandstones*, 67–78. https://doi.org/10.1002/9781444304237.ch5

Renard, F., Ortoleva, P., & Gratier, J. P. (1997). Pressure solution in sandstones: Influence of clays and dependence on temperature and stress. *Tectonophysics*, *280*(3–4), 257–266. https://doi.org/10.1016/s0040-1951(97)00039-5

Rutter, E. H. (1976). The kinetics of rock deformation by pressure solution. *Philosophical Transactions of the Royal Society of London,Series A*, *283*(1312), 203–219. https://doi.org/10.1098/rsta.1976.0079

Schimmel, M., Hangx, S., & Spiers, C. (2022). Effect of pore fluid chemistry on uniaxial compaction creep of bentheim sandstone and implications for reservoir injection operations. *Geomechanics for Energy and the Environment*, *29*, 100272. https://doi.org/10.1016/j.gete.2021.100272

Scholz, C. H. (1972). Static fatigue of quartz. *Journal of Geophysical Research*, *77*(11), 2104–2114. https://doi.org/10.1029/jb077i011p02104

Schutjens, P. M., Spiers, C. J., & Niemeijer, A. R. (2021). Surface microstructures developed on polished quartz crystals embedded in wet quartz sand compacted under hydrothermal conditions. *Scientific Reports*, *11*(1), 1–12.

Shengqi, Y., & Jiang, Y. (2010). Triaxial mechanical creep behavior of sandstone. *Mining Science and Technology*, *20*(3), 339–349. https://doi.org/10.1016/s1674-5264(09)60206-4

Shinohara, T., Jefferd, M., Spiers, C. J., & Hangx, S. J. (2024). The effect of strain rate on inelastic strain development in porous sandstones deformed under reservoir conditions. *International Journal of Rock Mechanics and Mining Sciences*, *184*, 105947. https://doi.org/10.1016/j.ijrmms.2024.105947

Spiers, C., De Meer, S., Niemeijer, A., & Zhang, X. (2003). Kinetics of rock deformation by pressure solution and the role of thin aqueous films. *Frontiers Science Series*, 129–158.

Torabi, A., Balsamo, F., Nogueira, F. C., Vasconcelos, D. L., Silva, A. C., Bezerra, F. H., & Souza, J. A. (2021). Variation of thickness, internal structure and petrophysical properties in a deformation band fault zone in siliciclastic rocks. *Marine and Petroleum Geology*, *133*, 105297. https://doi.org/10.1016/j.marpetgeo.2021.105297

van Noort, R., Visser, H. J., & Spiers, C. J. (2008). Influence of grain boundary structure on dissolution controlled pressure solution and retarding effects of grain boundary healing. *Journal of Geophysical Research*, *113*(B3), B03201. https://doi.org/10.1029/2007jb005223

Wiederhorn, S. (1974). Subcritical crack growth in ceramics. In *Fracture mechanics of ceramics* (pp. 613–646). Springer.

Wong, T., & Baud, P. (1999). Mechanical compaction of porous sandstone. *Oil and Gas Science and Technology*, *54*(6), 715–727. https://doi.org/10.2516/ogst:1999061

Wong, T.-f., David, C., & Zhu, W. (1997). The transition from brittle faulting to cataclastic flow in porous sandstones: Mechanical deformation. *Journal of Geophysical Research*, *102*(B2), 3009–3025. https://doi.org/10.1029/96jb03281

Zhang, R., Zhang, X., & Hu, S. (2015). Dissolution kinetics of quartz in water at high temperatures across the critical state of water. *The Journal of Supercritical Fluids*, *100*, 58–69. https://doi.org/10.1016/j.supflu.2015.02.010

Zhang, X., Spiers, C. J., & Peach, C. J. (2010). Compaction creep of wet granular calcite by pressure solution at 28°C to 150°C. *Journal of Geophysical Research*, *115*(B9). https://doi.org/10.1029/2008JB005853

Erratum

The originally published version of this article contained a typographical error. Figure 9 has been replaced to include the axis labels and numbers. This may be considered the authoritative version of record.